

Morphologic and molecular analysis of liver injury after SARS-CoV-2 vaccination reveals distinct characteristics

Sarp Uzun, Carl P. Zinner, Amke C. Beenen, Ilaria Alborelli, Ewelina M. Bartoszek, Jason Yeung, Byron Calgua, Matthias Reinscheid, Peter Bronsert, Anna K Stalder, Jasmine D Haslbauer, Juerg Vosbeck, Luca Mazzucchelli, Tobias Hoffmann, Luigi M. Terracciano, Gregor Hutter, Michael Manz, Isabelle Panne, Tobias Boettler, Maike Hofmann, Bertram Bengsch, Markus H. Heim, Christine Bernsmeier, Sizun Jiang, Alexandar Tzankov, Benedetta Terziroli Beretta-Piccoli and Matthias S. Matter

Table of Content

Supplementary material and methods.....	3
Fig. S1.....	18
Fig. S2.....	20
Fig. S3.....	22
Fig. S4.....	24
Fig. S5.....	26
Supplementary Table 1.....	28
Supplementary Table 2.....	29
Supplementary Table 3.....	30
Supplementary Table 4.....	31
Supplementary Table 5.....	32
Supplementary Table 6.....	34
Supplementary Table 7.....	34
Supplementary Table 8.....	34
Supplementary Table 9.....	35
Supplementary Table 10.....	36

Supplementary Table 11.....	37
Supplementary Table 12.....	38
Supplementary Table 13.....	38
Supplementary Table 14.....	38
Supplementary Table 15.....	39
Supplementary Table 16.....	40
Supplementary references.....	41

Supplementary Materials and Methods

Study design and patient selection

We collected six formalin-fixed and paraffin-embedded (FFPE) liver biopsy samples that showed liver injury after COVID-19 vaccination from the Institute of Pathology at the University Hospital Basel and the Institute of Pathology of Southern Switzerland in Locarno. For controls, we collected liver biopsies from patients with AIH (n = 9), alcoholic/non-alcoholic steatohepatitis (n = 17), and chronic hepatitis C viral infection with a high viral load (n = 13). Moreover, we included three patients with normal liver tissue by histology, who presented with a separate liver metastasis to the liver (2 with pancreatic carcinoma, 1 with urothelial carcinoma). For overlapping T-cell clone tracking, we additionally used the FFPE liver biopsy sample and blood samples of a published case “VILI patient Freiburg” (VILI_F).¹ For morphological comparison and multiplex immunohistochemistry, we collected liver biopsies from four drug-induced autoimmune-like hepatitis (DI-AILH). DI-AILH was caused in two patients by Infliximab and in two patients by Nitrofurantoin. All samples were evaluated by a consultant pathologist in the gastrointestinal/hepatology surgical pathologist team (MSM, JV, LT).

Clinical data collection

Reports included comprehensive laboratory and serological data that included anti-nuclear antibodies (ANA), anti-smooth muscle antibodies (SMA), anti-mitochondrial antibodies (AMA), anti-actin antibodies (AAA), anti-liver/kidney microsome type 1 (LKM-1), anti-liver cytosol type 1 (LC-1), anti-soluble liver antigen/liver pancreas antigen (anti-SLA/LP), anti-neutrophil cytoplasmic antibodies (ANCA), serum immunoglobulin G (IgG) and ceruloplasmin levels. Autoimmune liver serology was

evaluated according to local laboratory standards. Serological or PCR tests were performed for hepatitis virus A, B, C, D and E, Cytomegalovirus and Epstein–Barr virus.

Evaluation of liver injury

All patients were categorized for liver injury pattern by using the R-value, which is defined as serum alanine aminotransferase (ALT)/upper limit of normal (ULN) divided by serum alkaline phosphatase (ALP)/ULN. Liver injury was categorized as hepatocellular if the R ratio was >5 , as mixed if 2-5, and as cholestatic if <2 .²

Morphological evaluation of patient samples

Liver biopsies were evaluated by expert pathologists according to recommendations.³⁻

⁵ For Ishak grading, scores from 0-4 were assigned for periportal/periseptal interface hepatitis, focal spotty lytic necrosis/apoptosis/focal inflammation, and portal inflammation, while scores from 0-6 were assigned for confluent necrosis, as described.⁴ Fibrosis was staged from 0-6 according to the Ishak scoring system.⁴ The number of eosinophils in three lobules and portal tracts was counted and the following average number per lobule or portal tract was calculated.⁶ Fibrosis was classified according to the Ishak scoring system.⁴

Total RNA isolation from FFPE Tissue Samples

25-30 μm thick FFPE tissue sections were obtained from each patient, deparaffinized with xylene, and total RNA and DNA were extracted simultaneously with the AllPrep DNA/RNA FFPE Kit (Qiagen, 80234) following the vendor's instructions. Final DNA and RNA concentrations were measured with Qubit dsDNA HS Assay Kit (ThermoFisher, Q32851) and RNA HS Assay Kits (ThermoFisher, Q32852), respectively.

Total RNA isolation from Frozen Blood Sample

The blood sample of VILI patient #5 was collected into a PAXgene Blood RNA tube (Qiagen, 762165) from the time of liver biopsy (10 days after liver biopsy). RNA isolation was performed with PAXgene Blood RNA Kit (Qiagen, 762174) according to vendor's instructions. Final RNA concentration was measured with Qubit RNA HS Assay Kits (ThermoFisher, Q32852).

Bulk RNA-Sequencing and Transcriptome Analysis

Extracted RNAs were used for bulk RNA-sequencing with the HTG Transcriptome Panel (HTG Molecular Diagnostics). First, the samples and controls were randomized by HTG prior to the processing to reduce any potential intra-plate bias. Samples were processed in accordance with HTG EdgeSeq processing. Briefly, the nuclease protection probes (NPPs) were added to the lysed samples in the sample plate in excess amount and hybridized to the target mRNA. Then S1 nuclease was added to digest non-hybridized RNA and excess NPPs, thus producing a stoichiometric amount of target mRNA NPP duplexes. After the S1 digestion was completed, the processed sample was transferred to a new 96-well microtiter plate, referred to as the stop plate, and S1 digestion was terminated by the addition of a termination solution followed by heat denaturation of S1 enzyme. Each processed sample from the stop plate was used as a template for PCR reactions. The library was prepared by using a PCR with OneTaq (New England Biolabs) and EdgeSeq PCR tag primers (HTG Molecular Diagnostics). Next, the PCR clean-up procedures were performed with AMPure cleanup beads (Beckman Coulter). The library was then quantified with AccuClear fluorescent dye (Biotium) and a Molecular Devices SpectraMax plate reader. All samples processed within this study had sufficient PCR product to be pooled for

sequencing. The sequencing was performed on the Illumina NextSeq 550 sequencer in accordance with the manufacturer's recommendations but also included two HTG custom sequencing primers. The sequenced data was provided in the form of FASTQ files and aligned to the list of probes in the panel with the HTG EdgeSeq parser version 5.3.0.7148. The parsed data undergoes post sequencing quality control steps using the HTG Reveal software version 4.0. First, a sufficient quality and quantity of RNA is ensured by imposing that a maximum of four per cent of reads are attributed to the positive process control probes for each sample. Second, a minimum of seven million reads per sample is required for sufficient read depth. Third, samples with low expression variability are detected and excluded. These are defined as samples where the median $\log_2(\text{CPM})$ of negative control probes is greater than two.

Differential Expression Analysis

Differential analysis was performed in R with DESeq2 version 1.34.0.⁷ In accordance with the recommendation of HTG, the package's incorporated median of ratios normalization was used. The batches were inspected for unwanted variation using the RUVseq package (version 1.28). No significant correlation between batches and control signals could be found using a one-way ANOVA test. The normalized counts were prepared for visualization using a variance stabilizing transformation and further inspected for outliers in a principle component plot. One possible outlier was removed from the further analysis, completing the above cohort selection. A 3D principle component plot was created with Qlucore version 3.8 (Qlucore AB, Lund, Sweden) to explore the subgroups with optimal projection score for variance filtration. The differential expression itself was set up with a simple design formula containing only the variable of interest. Statistical significance was determined with the Wald test. Before the Benjamini-Hochberg false discovery rate adjustment, the number of genes

was automatically reduced by independent filtering. Additionally, the fold changes were adjusted with the apegglm shrinkage method.⁸ Heatmaps were generated with the R pheatmap package version 1.0.12 using complete linkage for hierarchical clustering and row scaling for better visual differentiation.

Gene Set Enrichment Analysis

For the gene set enrichment analysis, the pre-ranked log2 fold changes were compared to multiple databases using the fGSEA package version 1.20. The databases were obtained from MSigDB and are the Hallmark gene sets (h.all.v7.5.1.symbols.gmt.txt), the curated gene sets (c2.all.v7.5.1.symbols.gmt.txt) as well as the ontology gene sets (c5.all.v7.5.1.symbols.gmt.txt). For visualization, at most 30 significantly up or down regulated gene sets were first selected and the relevant ones were used for plotting. All significant gene sets were shared in **Supplementary Table 6**.

Cell Type Enrichment Analysis

The xCell package version 1.1.0 was used to estimate cell type enrichment. The algorithm is insensitive to normalization, but requires a gene length adjustment. This is automatically obtained by means of HTG's targeted probe approach. Hence the use of CPM normalized counts is justified. The package's list of identifiable cells was reduced to the populations occurring in the liver. The results were filtered additionally when the cell type was not present in at least two samples. The heatmap contains row scaled values with Ward D2 hierarchical clustering. Differences are tested with a rank sum test and adjusted for false rate discoveries.

Quantitative real-time PCR (qPCR)

Extracted RNAs from FFPE samples of VILI, AIH, and normal liver samples were used (described above in the **Total RNA isolation from FFPE Tissue Samples**). Complementary DNA (cDNA) was synthesized from total RNA with SuperScript VILO cDNA Synthesis Kit (Thermo Fisher, 11754250). qPCR was carried out using SYBR green dye (FastStart Universal SYBR Green Master, 4913914001). GAPDH was used as a reference gene. The relative expression of TSPAN8 and RNF-213 was calculated by the $2^{-\Delta\Delta C_t}$ method and the normal liver cohort was used as a control.⁹ The primer sets used in the study were included in **Supplementary Table 15**. The qPCR protocol was applied with the following incubation times: 50°C for 2 minutes; 95°C for 10 minutes; (95°C for 15 s/60°C for 1 min) × 40 cycles.

Spatial Transcriptomics with GeoMx Digital Spatial Profiler (DSP)

GeoMx DSP combines standard immunofluorescence techniques with digital optical barcoding technology to perform highly multiplexed, spatially resolved profiling experiments.¹⁰ DNA oligonucleotide probes were designed to bind mRNA targets. From 5' to 3', each probe is comprised of a 35- to 50-nucleotide target complementary sequence, an ultraviolet (UV) photo cleavable linker and a 66-nucleotide indexing oligonucleotide sequence containing a unique molecular identifier (UMI), RNA ID sequence and primer binding sites.

Three FFPE tissue sections of 5-μm from liver biopsy tissue microarray (TMA) with VILI (n=6) and AIH (n=8) (TMA construction described below in the **Immunoprofiling with CO-Detection by indEXing (CODEX)**) were mounted on positively charged histology slides. Sections were incubated at 65 °C for 1 hour. Then, sections were deparaffinized in 3 xylol baths of 5 minutes and rehydrated in ethanol gradient from

100% EtOH 2 baths of 5 minutes, followed by 95% EtOH 5 minutes. Slides were then washed in 1X PBS. Antigen retrieval was carried out with Tris-EDTA pH 9.0 buffer at 100°C for 20 minutes at low pressure. Slides were first immersed into hot water for 10 seconds and then immersed into Tris-EDTA buffer. The cooker vent kept open during the procedure to ensure low pressure and it was allowed to reach 100°C. Slides were then washed with 1X PBS, and incubated in proteinase K containing PBS (1ug/ml) for 15 minutes at 37°C and washed again in 1X PBS. Tissue were post-fixed in 10% neutral-buffered formalin (NBF) for 5 minutes, washed two times 5 minutes in NBF stop buffer (0.1M Tris Base, 0.1M Glycine) and finally one time in 1X PBS. The mix of Whole Transcriptome Atlas probes (WTA, Nanostring) was dropped on each section and covered with HybriSlip Hybridization Covers. Slides were then incubated for hybridization overnight at 37°C in a Hyb EZ II hybridization oven (Advanced cell Diagnostics). The day after, HybriSlip covers were gently removed and 25 minutes stringent washes were performed twice in 50% formamide and 2X saline sodium citrate (SSC) at 37 °C. Tissues were washed for 5 min in 2× SSC, then blocked in Buffer W (Nanostring Technologies) for 30 min at room temperature in a humidity chamber. Next, 500 nM Syto83 and antibodies targeting CD3 (BioRad, clone CD3-12), CD20 (Novus, clone IGEL/773) and Arginase (Cell Signaling, clone D4E3M) in Buffer W were applied to each section for 1 h at room temperature. Slides were washed twice in fresh 2× SSC then loaded on the GeoMx DSP.

Entire slides were imaged at ×20 magnification and morphologic markers were used to select Region Of Interest (ROI) either using circle or organic shapes. Automatic segmentation of ROI based on Arginase+ markers were used to defined Area of Illumination (AOIs). This allowed to separate liver cells (Arginase+) and cells around liver. A total of 59 AOIs were exposed to 385 nm light (UV), releasing the indexing oligonucleotides which were collected with a microcapillary and deposited in a 96-well

plate for subsequent processing. The indexing oligonucleotides were dried down overnight and resuspended in 10 µl of DEPC-treated water.

Sequencing libraries were generated by PCR from the photo-released indexing oligos and AOI-specific Illumina adapter sequences, and unique i5 and i7 sample indices were added. Each PCR reaction used 4 µl of indexing oligonucleotides, 4 µl of indexing PCR primers, 2 µl of Nanostring 5X PCR Master Mix. Thermocycling conditions were 37 °C for 30 min, 50 °C for 10 min, 95 °C for 3 min; 18 cycles of 95 °C for 15 s, 65 °C for 1 min, 68 °C for 30 s; and 68 °C for 5 min. PCR reactions were pooled and purified twice using AMPure XP beads (Beckman Coulter, A63881), according to the manufacturer's protocol. Pooled libraries were single-sequenced at 27 base pairs and with the single-index workflow on an Illumina NovaSeq S4 instrument. FastQ files were converted into DCC files according to manufacturer's pipeline. Digital Count Conversion files were imported back into the GeoMx DSP instrument for QC and data analyses using GeoMx DSP analysis suite version 2.4.2.2 (Nanostring).

GeoMx DSP Differential Expression Analysis and Gene Set Enrichment Analysis

Following standard preprocessing and quality control of data as outlined by NanoString guidelines, differential gene expression analysis was performed on the quantile normalized count data in R with limma version 3.52.4. The simple design model was set up to compare ROIs between our VILI and AIH cohorts, taken across portal and central regions of the liver. Statistical significance was determined using an empirical Bayes t-test, as described by the limma package. All P-values were adjusted using Benjamini-Hochberg. A full list of differentially expressed genes can be accessed in **Supplementary Table 7**.

For gene set enrichment analysis, pre-ranked log2 fold change values were mapped to MSigDB gene sets using fgsea version 1.22.0. The same aforementioned gene sets used in our analysis of bulk transcriptomic profiling were used here (hallmark, curated, and ontology gene sets). To visualize pathways and confirm our findings, the same enriched pathways plotted in our bulk RNA-sequencing analysis are also pulled and plotted from the GeoMx dataset. All significant gene sets are shared in **Supplementary Table 8**.

PBMC Isolation, Enrichment of spike-specific CD8⁺ T cells and RNA Isolation from Blood Samples of VILI_F

PBMCs (Peripheral blood mononuclear cells) were isolated with density gradient centrifugation from anticoagulated blood samples of patient VILI_F which were collected from three different time points. SARS-CoV-2 spike peptide (S378-386: KCYGVSP TK) was synthesized (Genaxxon Bioscience), loaded on HLA-A*03:01 easYmers® (immunAware) and subsequently conjugated with phycoerythrin (PE)-streptavidin (Agilent). PBMCs were incubated with phycoerythrin (PE)-conjugated tetramerized S378-386-loaded HLA-A*03:01 easYmers as described before.¹ Virus-specific CD8⁺ T-cells were enriched by MACS technology using anti-PE beads. The remaining CD8⁺ T-cells which were depleted from Spike (A*03/S378)-specific CD8⁺ T-cells were used for TCR sequencing. For this, total RNA was isolated from CD8⁺ T-cells with AllPrep DNA/RNA Mini Kit (Qiagen, 80204) according to vendor's instructions.

T-Cell Receptor (TCR) and B-Cell Receptor (BCR) Library Preparation and Sequencing

RNAs extracted from FFPE samples of VILI and AIH, from frozen blood sample of VILI patient #5 and from CD8⁺ T-cells of VILI_F were used to prepare the libraries for TCR and BCR sequencing. cDNA was synthesized from RNA by using the SuperScript VILO cDNA Synthesis Kit (Invitrogen, 11754250) and Ion Torrent NGS Reverse Transcription Kit (ThermoFisher, A45003) for TCR and BCR sequencing, respectively. T-cell and B-cell RNA was quantified by qPCR with TaqMan Gene Expression Assay, CD247 (20X, Hs00167901_m1) and CD19 (20X, Hs01047413_g1). Final input was normalized to 1 ng of T- and B-cell derived RNA per sample. For samples with low T- and B-cell counts, maximum RNA input was loaded for library preparation. Next-Generation Sequencing (NGS) libraries were prepared using the Oncomine TCR Beta-SR RNA Assay (ThermoFisher, A39359) and the Oncomine BCR IGH SR RNA Assay (ThermoFisher, A45484) according to manufacturer's instructions. Amplified and barcode ligated libraries were purified with AMPure XP Reagent (Beckman Coulter, A63880) and quantified with the Ion Universal Library Quantitation Kit (ThermoFisher, A26217). The library pool was prepared by combining equal volumes of libraries at 50 pmol/L concentration and loaded into Ion 550™ Chip (ThermoFisher, A34537). The libraries were sequenced on an Ion GeneStudio S5 Prime Sequencer (ThermoFisher).

TCR and BCR Sequencing Data Analysis

Sequencing analysis was performed on Ion Reporter Software, Version 5.18 (ThermoFisher). General immune repertoire metrics such as Shannon diversity index and evenness were calculated to describe the diversity of the T- and B-cell clones in the tissues. Shannon diversity index (H) of each patient was defined with the formula:

$$H = - \sum_{i=1}^N P_i \log_2 (P_i)$$

where the sum is taken over N number of different clones and P_i is the frequency of the clone i . Evenness, which has values between 0 and 1, denotes the distribution of T-/B-cell clones in a single sample. Values close to 0 indicate an unbalanced clone distribution with dominant high-frequency clones, while values close to 1 indicate a balanced distribution of clones.¹¹ Total clonal space analysis of T- and B-cell clones was done by frequency classification of T- and B-cell clones according to their ranked abundance in the total immune repertoire in each sample. The clonal space was divided into top 1%, top 1-2%, top 2-5%, and top >5% as shown previously^{11, 12} and the total frequency of each clonal space was calculated by summing up the frequency of each clone found in the respective space. Each T-cell with the same variable-joining regions and complementarity-determining region 3 (CDR3) is defined as a T-cell clone. Shared T-cell clone analysis between samples was performed with the R Studio Stringdist package¹³ by calculating the Levenstein distance between CDR3 amino acid sequences. TCR convergence was defined as T-cells with identical TCRs and the same amino acid sequences but with different nucleotide sequences. CDR3 nucleotide length distribution of T- and B-cell clones were plotted with R Studio Version 4.1.2. ggplot 2.¹⁴ The heatmap for TCR beta chain variable-joining gene (TRBV-J) and Ig heavy chain variable-joining gene (IGHV-J) usage was generated by using the frequency of each T-cell or B-cell clone in the VILI or AIH patient. For plotting, R pheatmap package version 1.0.12 was used with row scaling for better visual differentiation. For epitope prediction, TCR CDR3 β amino acid sequences from VILI cases were uploaded into a web-based epitope prediction tool (<http://tools.iedb.org/tcrmatch/>). Highest match prediction (>0.97) was selected as the filtering level and CDR3 β -matching spike glycoprotein epitopes were summarized in **Supplementary Table 11**.

Immunoprofiling with CO-Detection by indEXing (CODEX)

We reconstructed two tissue blocks by using the FFPE samples of VILI and AIH, with normal liver and tonsils as controls. First, tissue blocks were melted and approximately 0.5 mm of tissue was cut from each liver needle biopsy sample. Then, these biopsy sample pieces were aligned next to each other and re-embedded into two tissue blocks. From each tissue block, two 4µm sections were taken on poly-L-lysine coated coverslips for multiplex immunohistochemistry and one 2 µm section for H&E. Tissue sections were stained according to the protocol supplied by the manufacturer (Akoya Biosciences, CODEX User Manual Rev C) with slight modifications. For heat-induced epitope retrieval, tissue sections were incubated in citrate buffer (pH: 6.0) for 15 minutes at 98°C in a laboratory-type microwave. The tissue sections were incubated with the primary antibody cocktail for 3 hours at room temperature. The tissues were fixed with 1.6% PFA for 10 minutes, 100% methanol for 5 minutes, and CODEX fixative reagent for 20 minutes. Stained tissues were stored in the storage buffer at 4°C until image acquisition. The image acquisition was done with a Leica DMI8 microscope with a 20x objective (HC Plan-Apo 20x/0.8Air) with a Prime 95B camera and Leica LAS X Software Version 5.1.0. Data was acquired with 9 Z-steps of 1.5 µm. For focus setup, a focus map was created by selecting 5-7 focus points per tissue and using autofocus mode. The reagents and antibodies used in the CODEX were listed in **Supplementary Table 16**.

CODEX Data Preprocessing

Fiji¹⁵ was used for image preprocessing. Briefly, images from a single tile were collected (including all 4 channels and 9 Z-steps) and a rolling ball subtraction with a radius of 15 pixels was performed. The z-stack was maximum projected for each channel separately. A registration of cells between consecutive cycles based on DAPI

(4',6-diamidino-2-phenylindole) was performed using MultiStackReg plugin¹⁶ and the same correction was propagated on the remaining channels. Tiles were stitched using Grid/Collection stitching plugin.¹⁷ Due to high autofluorescence in the liver tissue, blank cycles (only DAPI channel without another staining with the same exposure time in the corresponding channels) were acquired and subtracted from the remaining cycles.

CODEX Data Analysis

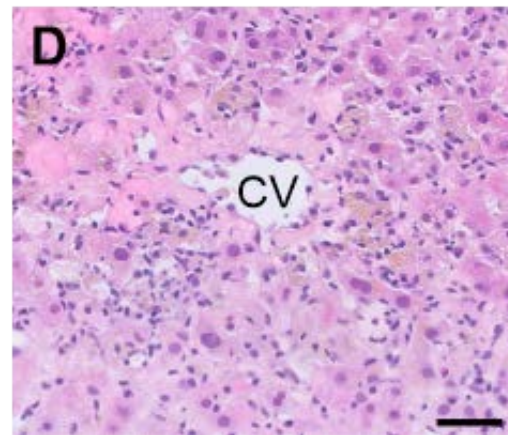
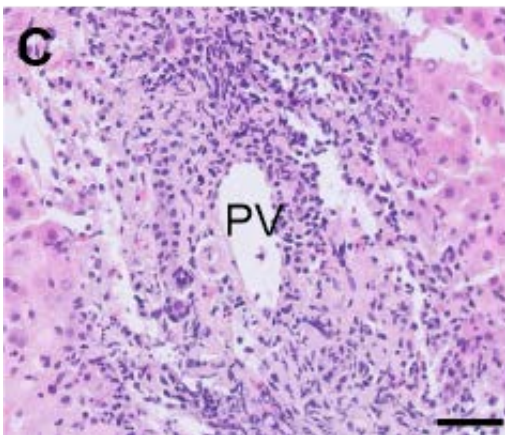
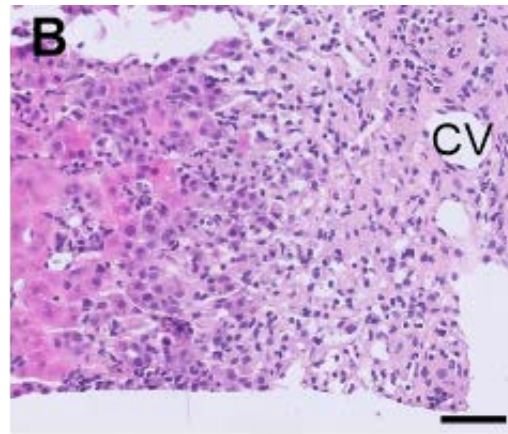
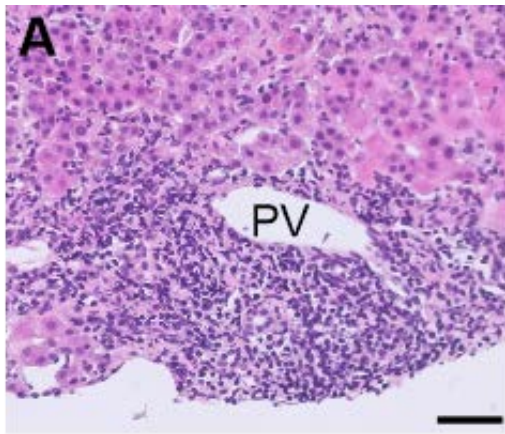
Multichannel tiff was further saved as a pyramidal file using the Kheops plugin¹⁸, and the image was opened in QuPath.¹⁹ Stainings were validated by visual inspection and from the proteinaatlas.²⁰ Tonsils and normal liver were used for the staining validation and were not included in the data analysis. Cell segmentation was done on nuclear channel DAPI using StarDist2D²¹ plugin within QuPath with the following parameters: probability threshold: 0.7, pixel size: 0.5 and cell expansion: 2.0 using the model dsb2018_heavy_augment.pb. A table with the mean intensity of each marker per cell was exported and further used in OMIQ software (<https://omiq.ai>). Single-cell data was clustered using Phenograph algorithm²² with k=20 into 51 phenotypes. Clustering was based on the following markers: arginase, CD3, CD4, CD8, CD20, CD68, CD79a, CK19, FoxP3, and Ki67. To validate clusters, each cell was color-coded based on its cluster-ID, overlaid on a multichannel image, and visually inspected. Clusters with similar expression patterns after visual verification were merged and, additionally, clusters with unspecific staining were excluded. The final number of clusters was 11. Portal and central veins were annotated on the tissue based on CD31 from fluorescent staining and corresponding H&E image. Those regions were expanded by 150 µm to delineate portal and central vein regions. Distance from each cell to the nearest annotation was calculated.

The antibody panel for DI-AILH consisted of 9 antibodies to evaluate immune cell composition within portal and centrilobular regions. QuPath¹⁷ was used to train object classifiers based on cell features such as mean, minimum, maximum, standard deviation of intensity values. One classifier was trained to distinguish CD8⁺, CD4⁺, CD79a⁺ cells, separate classifiers were trained for CD3⁺ and Foxp3⁺ cells. Composite classifier was applied to extract different cell types.

All data were analyzed on raw pixel values and brightness and contrast were adjusted for visualization. Final figures were prepared using Fiji.

Statistical Analysis

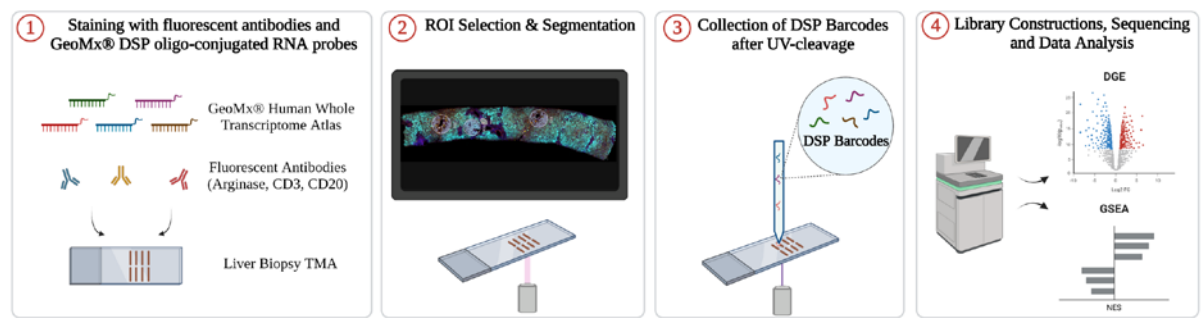
The data were represented as mean and standard error of mean or median and min-max values. Unpaired two-tailed Student *t*-test and Wilcoxon rank-sum test was used for two group comparisons. Spearman rank correlation test was used for all correlation analyses. The statistical tests were specified in the respective figure legend. A two-tailed *p* value < 0.05 was used to infer statistical significance. All graphs and statistical testing were done using GraphPad Prism version 9.2.0 and R Studio Version 4.1.2.



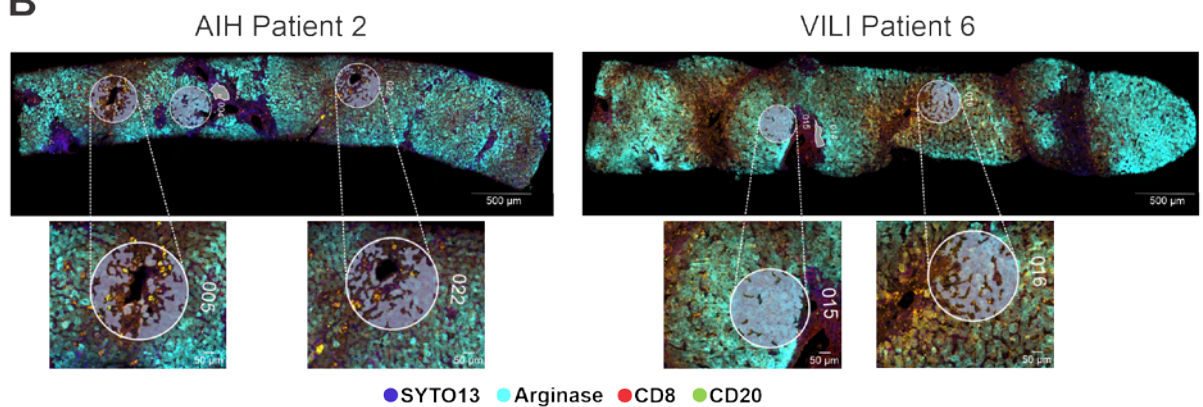
Supp. Fig 1. Representative image showing liver morphology from VILI and AIH.

(A) Portal tract of VILI and **(C)** AIH with portal inflammation and interface hepatitis. **(B)** Extensive centrilobular necrosis of VILI and **(D)** less pronounced centrilobular necrosis of AIH, both with intralobular inflammation. PV = portal vein, CV = central vein. Bar = 50 μ m.

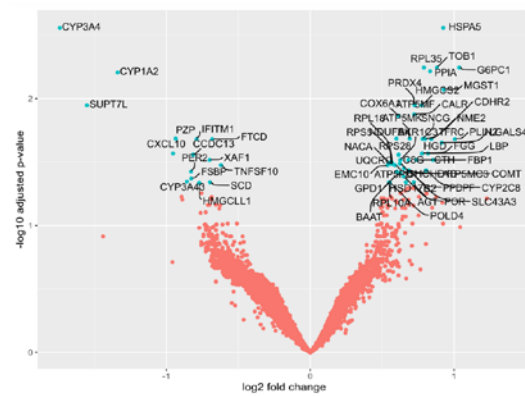
A



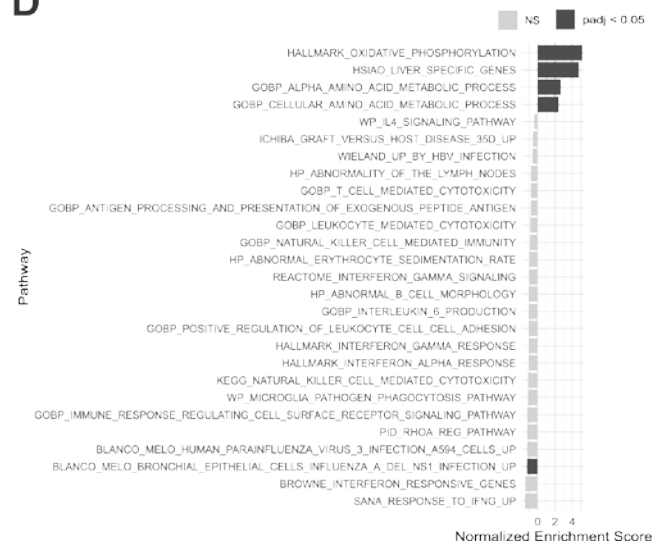
B



C



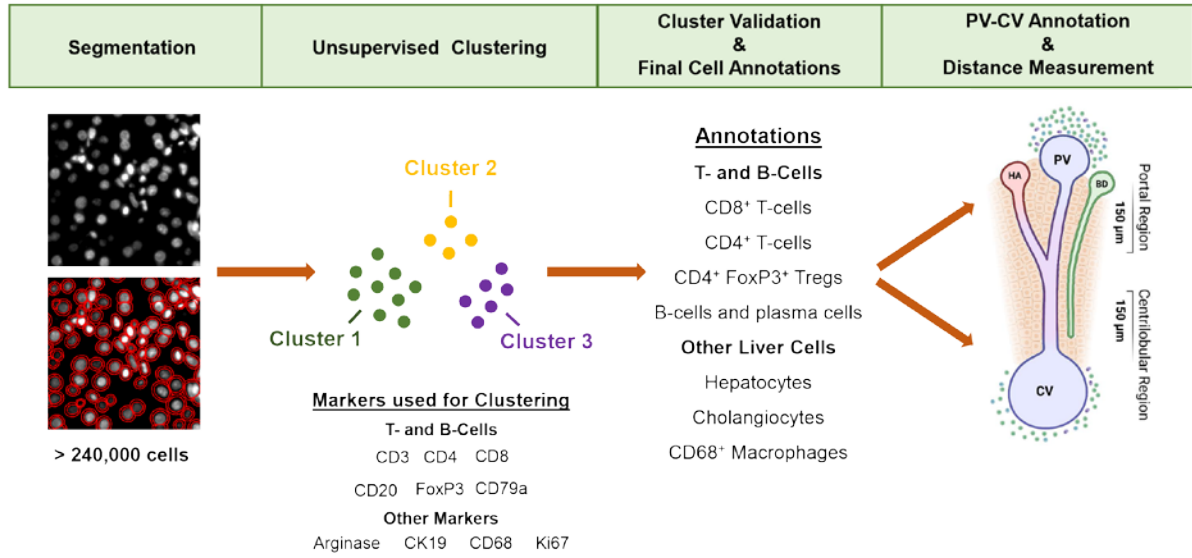
D



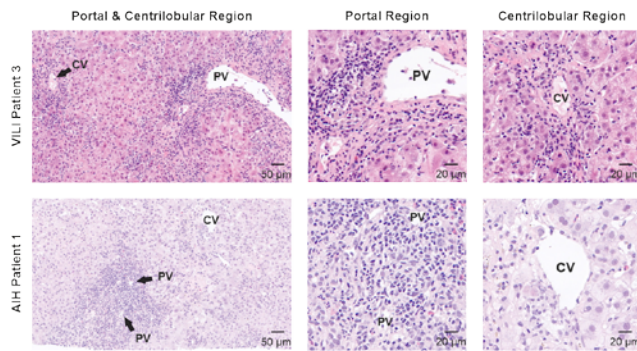
Supp. Fig 2. Spatial Transcriptomics of VILI and AIH Patient Samples

(A) GeoMx workflow. The figure was created in BioRender.com (2023) **(B)** 59 ROIs were selected from 3 different tissue microarrays (TMAs) having VILI (n=6) and AIH (n=8) biopsy samples. Automatic segmentation of Arginase⁺ cells in ROIs was performed. Bar=500 μ m for whole liver biopsy; bar=50 μ m for ROIs **(C)** Volcano plot shows the differentially expressed genes between VILI and AIH hepatocytes **(D)** Hepatocytes from VILI show significant enrichment of oxidative and metabolic pathways. Only pathways that were visualized in the bulk-RNA-sequencing enrichment analysis are presented.

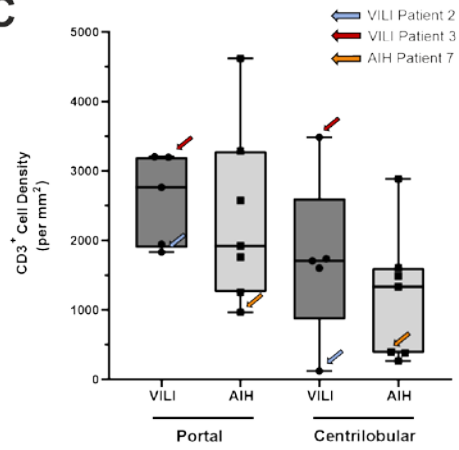
A



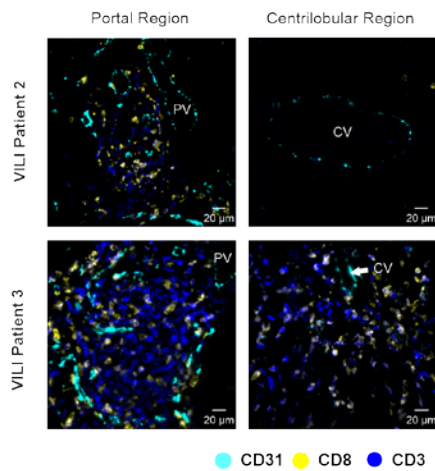
B



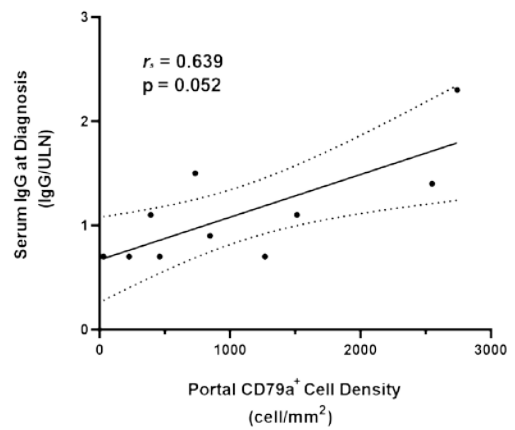
C



D



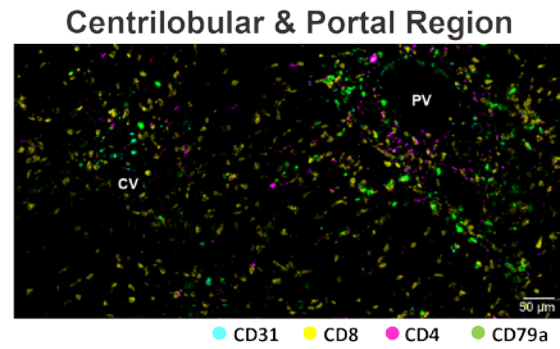
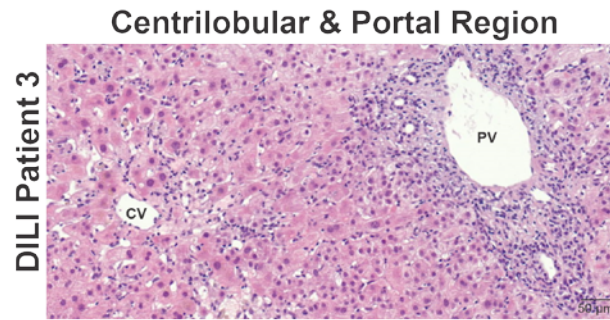
E



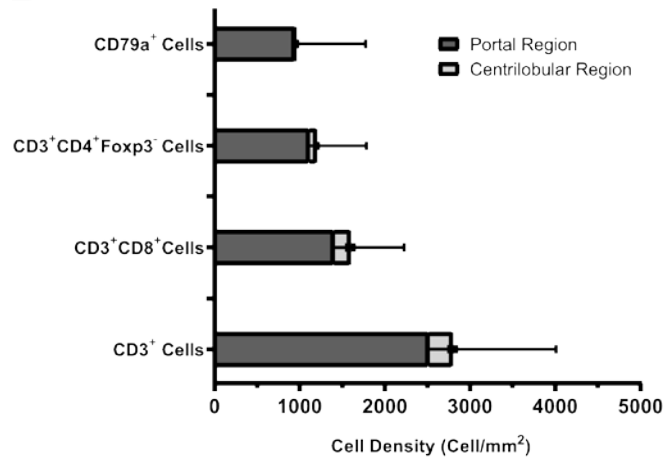
Supp. Fig. 3. CODEX Analysis of VILI and AIH Patient Samples

(A) CODEX data analysis workflow. CV: central vein; PV: portal vein, HA: hepatic artery, BD: Bile duct. A part of the figure was adapted from “hepatic sinusoid”, by BioRender.com (2022). **(B)** Hematoxylin and eosin staining of portal and centrilobular region of VILI patient #3 and AIH patient #1. CV: central vein; PV: portal vein. **(C)** CD3⁺ cell density in the portal and centrilobular region of VILI and AIH patients. Blue arrows indicate VILI patient #2, red arrows indicate VILI patient #3, orange arrows indicate AIH patient #7. **(D)** CD3⁺ and CD3⁺ CD8⁺ cell distribution in the portal and centrilobular region of VILI and AIH patients. Cyan(CD31), blue(CD3), yellow(CD8). CV: central vein; PV: portal vein. **(E)** Correlation analysis between IgG serum level at diagnosis (IgG/ULN) and portal B-cell (CD79a⁺) density. The black line shows the linear regression line and dotted lines represent the 95% confidence interval upper and lower limits (Spearman rank correlation test). VILI cohort, $n=5$; AIH cohort, $n=7$. Each dot represents a patient.

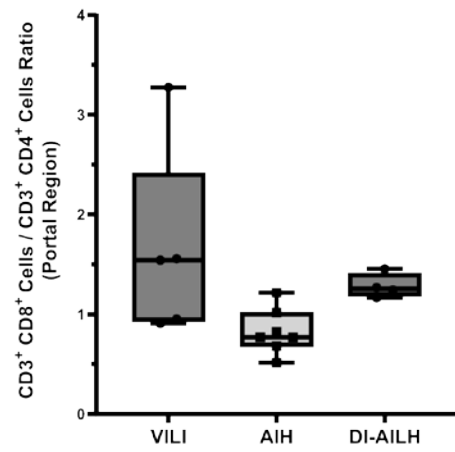
A



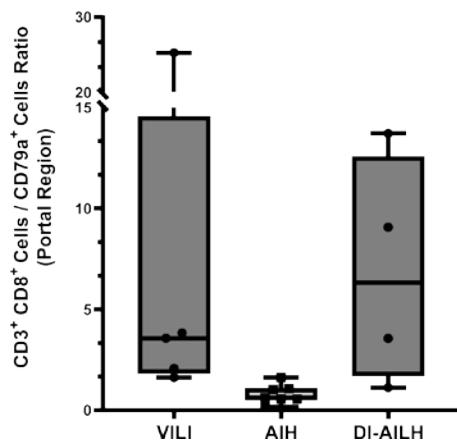
B



C



D



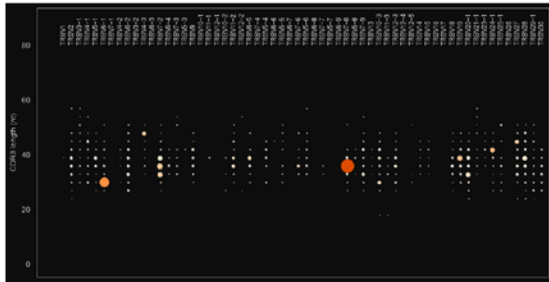
Supp. Fig. 4. CODEX Analysis of DI-AILH

(A) H&E and CODEX staining of portal and centrilobular region of DI-AILH patient #3. CV: central vein; PV: portal vein. Cyan (CD31), yellow (CD8), pink (CD4) and Green (CD79a⁺). **(B)** Immune cell distribution in the portal and centrilobular region of DI-AILH samples. Bar graphs indicate mean and standard error of mean (SEM) of immune cell densities (cells/mm²). **(C)** Ratio of CD3⁺ CD8⁺/CD3⁺ CD4⁺ T cells in the portal region of VILI, AIH and DI-AILH samples. **(D)** Ratio of CD3⁺ CD8⁺/CD79a⁺ T cells in the portal region of VILI, AIH and DI-AILH samples.

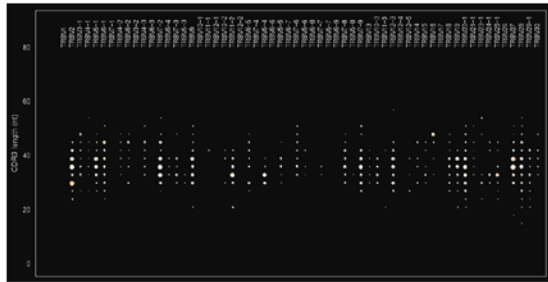
A

TCR Spectratyping Plots

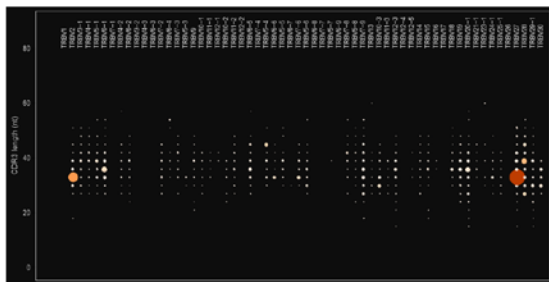
VILI Patient 2



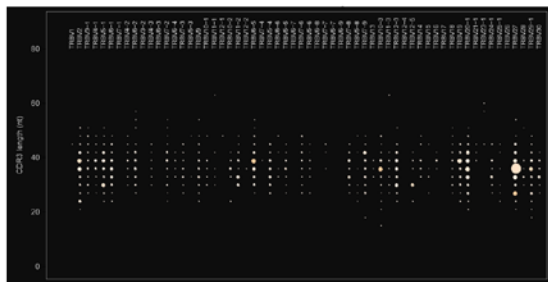
AIH Patient 2



VILI Patient 6



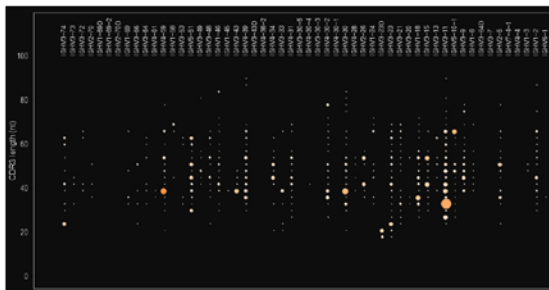
AIH Patient 3



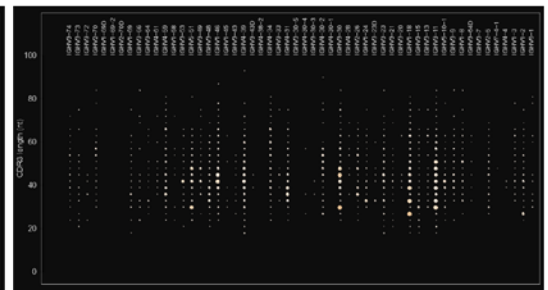
B

BCR Spectratyping Plots

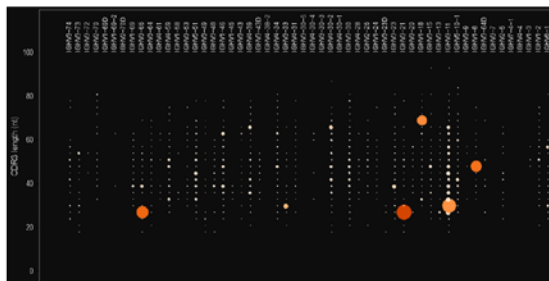
VILI Patient 2



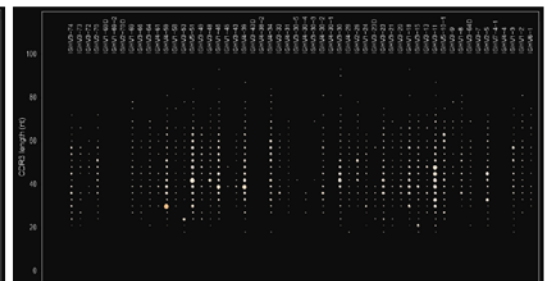
AIH Patient 2



VILI Patient 6



AIH Patient 3



Supp. Fig. 5. TCR and BCR Repertoire Spectratyping Plots from Two VILI and AIH Patients

(A) TCR repertoire spectratyping plots of two VILI (#2, #6) and two AIH (#2, #3) patients. The x-axis shows different TCR- β chain V genes and the y-axis shows different CDR3 nucleotide lengths. **(B)** BCR repertoire spectratyping plots of two VILI (#2, #6) and two AIH (#2, #3) patients. The x-axis shows different IgH-V genes and the y-axis shows different CDR3 nucleotide lengths. Circle size indicates the frequency of a particular variable gene-CDR3 nucleotide length combination and circle color indicates the frequency of the largest clone among other clones having the same variable gene-CDR3 nucleotide length combination.

Supplementary Table 1. Comparison of clinical and morphological features of VILI and AIH patients

	VILI (n = 6)	AIH (n = 9)	<i>p</i> value VILI vs AIH
Age, median years (range)	58 (21-85)	61 (49-78)	n.s. (0.76)
Gender (female), n (%)	2 (33%)	8 (89%)	
AST/ULN, mean	38.3	18.0	ns (0.08)
ALT/ULN, mean	44.1	27.7	ns (0.30)
GGT/ULN, mean	5.3	7.6	ns (0.33)
ALP/ULN, mean	1.2	1.5	ns (0.43)
R-value, mean	44.0	19.2	ns (0.11)
Bilirubin/ULN, mean	9.2	4.0	ns (0.13)
Pattern of injury			
• Hepatocytic % (n)	100% (n = 6)	88.9% (n = 8)	
• Mixed	0	11.1% (n = 1)	
• Cholestatic	0	0	
elevated ANA and/or ASMA/AAA, % (n)	67% (4)	100% (9)	
anti-SLA, anti-LKM1, or anti-LC1	0	0	
AMA	1*	0	
ANCA	0	2	
Increased IgG, n/totally measured (%)	2/5 (40%)	4/8 (50%)	
Ishak Grading, score, mean	12.2	10.3	ns (0.34)
• Piecemeal necrosis	2.3	2.9	ns (0.39)
• Focal lytic necrosis/apoptosis/inflammation	3.7	3.4	ns (0.63)
• Portal inflammation	2.3	3.1	ns (0.16)
• Confluent necrosis	3.8	1	0.0025
Fibrosis			
• F0	6 (100%)	5 (55.5%)	
• F1	0	4 (44.4%)	
Eosinophils portal tract (mean/HPF)	30.0	57.8	ns (0.21)
Eosinophils lobular (mean/HPF)	11.8	12.1	ns (0.96)
Simplified AIH score ≥ 6	60% (3/5)	100 % (9/9)	

Abbreviations: AAA: anti-actin antibodies, ALP: alkaline phosphatase, ALT: alanine aminotransferase, AMA: anti-mitochondrial antibody, ANA: anti-nuclear antibody, ANCA: Anti-neutrophil cytoplasm antibodies, Anti-LC1: anti-liver cytosol type 1, Anti-LKM1: anti-liver-kidney microsome 1, Anti-SLA: anti-soluble liver antigen, ASMA: anti-smooth muscle antibody, AST: aspartate aminotransferase, GGT: Gamma-glutamyltransferase, HPF: high power field. Two-group comparison: unpaired student *t*-test. ns: not significant. *not classical AMA

Supplementary Table 2. Clinical Features of VILI and AIH patients

Supplementary Table 2 can be found as a separate supplementary document.

Supplementary Table 3. Morphological Evaluation of VILI and AIH Samples

Patient ID	Time between symptoms and liver biopsy (days)	Ishak Staging (Fibrosis)	Ishak Grading Total	Ishak Grading	Interface hepatitis (0-4)	Confluent necrosis (0-6)	Focal lytic necrosis (0-4)	Degree of Portal inflammation (0-4)
VILI1	11	0	16	4+5+4+3	4	5	4	3
VILI2	2	0	3	0+0+2+1	0	0	2	1
VILI3	11	0	16	4+5+4+3	4	5	4	3
VILI4	90	0	11	1+4+4+2	1	4	4	2
VILI5	16	0	14	3+5+4+2	3	5	4	2
VILI6	77	0	13	2+4+4+3	2	4	4	3
AIH1	9	0	14	4+2+4+4	4	2	4	4
AIH2	60	1	11	3+0+4+4	3	0	4	4
AIH3	150	0	10	3+0+4+3	3	0	4	3
AIH4	30	0	14	4+2+4+4	4	2	4	4
AIH5	120	0	12	3+2+4+3	3	2	4	3
AIH6	n.a.	1	6	2+0+2+2	2	0	2	2
AIH7	90	0	6	2+0+2+2	2	0	2	2
AIH8	n.a.	1	9	2+1+4+2	2	1	4	2
AIH9	90	1	11	3+2+3+3	3	2	3	3

Supplementary Table 4. Cohort of patients with chronic hepatitis C infection, ASH or normal liver

Number Publication	Sex	Age	Metavir_Fibrosis	Metavir_Activity	AST (U/L)	ALT (U/L)	GGT (U/L)	ALP (U/L)	Bilirubin TOT umol/l,
HCV1	m	66	F4	A3	NA	NA	NA	NA	NA
HCV2	m	53	F4	A3	109	103	242	78	7
HCV3	f	62	F4	A2	76	85	45	33	21
HCV4	m	64	F4	A3	134	132	179	70	13
HCV5	m	70	F4	A2	NA	NA	NA	NA	NA
HCV6	m	67	F4	A3	93	105	83	66	22
HCV7	m	53	F4	A3	44	41	149	105	7
HCV8	f	51	F4	A3	88	82	82	62	9
HCV9	m	46	F4	A3	127	166	66	56	10
HCV10	m	64	F4	A2	106	150	96	51	12
HCV11	f	56	F4	A3	126	126	58	83	15
HCV12	m	53	F4	A3	113	122	234	118	20
HCV13	m	61	F4	A3	35	44	152	94	13
ASH1	f	65	F4	A2	55	36	65	125	21
ASH2	m	65	F4	A2	36	16	62	41	53
ASH3	m	64	F4	A1	51	38	313	192	7,7
ASH4	m	78	F4	A1	60	54	274	117	21,9
ASH5	f	64	F4	A1	37	26	293	98	30,1
ASH6	m	80	F4	A2	74	45	61	158	80,9
ASH7	m	56	F4	A1	78	47	235	168	19,2
ASH8	f	61	F4	A1	NA	NA	NA	NA	NA
ASH9	f	73	F4	A1	NA	NA	NA	NA	NA
ASH10	f	73	F4	A1	25	34	141	47	8,2
ASH11	m	69	F4	A1	42	36	173	59	13,4
ASH12	f	70	F4	A1	59	66	337	110	13,6
ASH13	f	63	F4	A1	35	29	382	213	7
ASH14	f	48	F4	A1	163	66	181	119	282
ASH15	m	50	F4	A1	580	83	119	70	111,7
ASH16	m	72	F4	A1	93	44	104	131	20,4
ASH17	f	65	F4	A2	NA	NA	NA	NA	NA
Normal1 *	f	46	F0	A0	10	6	76	111	3.4
Normal2 †	f	70	F0	A0	61	50	367	351	10.6
Normal3 †	m	74	F0	A0	42	13	511	439	17.7

* Metastasis of a urothelial carcinoma, normal liver histology

† Metastasis of a pancreas carcinoma, normal liver histology

Abbreviations: f: female, m: male, ALP: alkaline phosphatase, ALT: alanine aminotransferase, AST: aspartate aminotransferase, GGT: Gamma-glutamyltransferase, NA: not available, TOT: total, ASH: alcoholic steatohepatitis.

Supplementary Table 5. Genes with significant differential expression between VILI and AIH cohorts after bulk RNA sequencing

gene	baseMean	log2FoldChange	lfcSE	pvalue	padj
ABCA5	543.8661421	0.7730	0.3282	0.0008	0.0473
ABI3	565.7659818	-1.0031	0.2948	0.0000	0.0102
ARG1	17209.79428	0.9776	0.3322	0.0002	0.0259
ARHGAP26	399.3413445	-0.8445	0.3090	0.0002	0.0272
ARHGAP4	543.7854154	-1.0131	0.3802	0.0002	0.0272
ATL2	1598.865463	0.5829	0.1631	0.0000	0.0102
ATP5MD	6643.073467	0.6299	0.2390	0.0005	0.0370
BTN3A3	690.6819673	-0.8072	0.2999	0.0003	0.0273
C19orf33	18862.62998	0.6973	0.2550	0.0003	0.0310
CD99	4145.558182	1.2671	0.2797	0.0000	0.0019
CSK	666.261223	-0.6731	0.2784	0.0006	0.0414
DCTN6	858.4521553	0.7393	0.2068	0.0000	0.0102
EBPL	1304.140801	0.9047	0.2980	0.0001	0.0237
EPHB4	1456.347616	0.6296	0.2070	0.0001	0.0256
FAM229B	586.6193901	0.8230	0.3386	0.0007	0.0431
FIS1	451.1944193	-0.6963	0.2542	0.0003	0.0273
GATAD2B	423.9286002	-0.5937	0.2486	0.0008	0.0453
GBP3	1294.260635	-0.9089	0.3278	0.0002	0.0272
GDA	894.3891478	0.7796	0.2877	0.0003	0.0310
H3-5	353.4044039	-0.8586	0.3814	0.0007	0.0444
HAL	1139.962025	1.2623	0.4194	0.0001	0.0237
HEBP2	3014.700053	0.8674	0.2335	0.0000	0.0102
HGD	9254.483218	0.7722	0.3184	0.0007	0.0444
HOOK1	1366.537432	0.8817	0.2500	0.0000	0.0102
IFITM2	2016.331952	0.7132	0.2403	0.0002	0.0259
INPP4A	553.5798021	-0.8775	0.2433	0.0000	0.0102
INPP5D	372.1520739	-0.8205	0.3449	0.0006	0.0399
INSIG1	4013.458116	1.1973	0.3794	0.0001	0.0227
IRF1	1693.638604	-0.8191	0.3019	0.0002	0.0272
KDM5C	530.7694426	-0.8084	0.2742	0.0001	0.0237
LCLAT1	543.3195653	0.6482	0.2276	0.0002	0.0273
LOC101060341	1003.839707	-0.8011	0.3027	0.0003	0.0294
LOC102724971	16769.75507	-1.2340	0.5823	0.0007	0.0444
MRPS22	1230.668932	0.5804	0.2083	0.0003	0.0310
NFIC	7714.168296	0.6182	0.1933	0.0001	0.0227
NOSTRIN	415.3506798	0.7809	0.2935	0.0004	0.0330
NSD3	581.4232978	-0.6190	0.2474	0.0005	0.0385
NUCB2	1335.339463	0.8192	0.2277	0.0000	0.0102
ORC4	536.7131975	0.6807	0.2410	0.0003	0.0273
OXLD1	562.7979355	0.6239	0.2558	0.0008	0.0460
PARP14	1296.769804	-0.6581	0.2267	0.0002	0.0259
PGRMC2	4957.914803	0.5999	0.2333	0.0006	0.0399
PIGP	1112.986821	0.6031	0.2109	0.0003	0.0273
PLPP1	1944.667587	0.6116	0.2354	0.0005	0.0383

POLR2J	4907.159313	0.5971	0.2204	0.0004	0.0345
PRF1	319.5159479	-1.0617	0.4514	0.0005	0.0380
PSME2	1921.837718	-0.7045	0.2340	0.0001	0.0237
RGPD_Family	937.2468403	0.6356	0.2078	0.0002	0.0259
RNF213	1170.049883	-0.7985	0.2658	0.0001	0.0237
RTL8A	1651.651326	0.8062	0.2247	0.0000	0.0102
SAA_Family	39655.04827	3.3748	0.8766	0.0000	0.0102
SAA1	18281.59568	3.1488	0.8607	0.0000	0.0102
SCML1	474.779273	0.7891	0.2690	0.0002	0.0259
SGK2	1216.511862	0.6762	0.2257	0.0002	0.0259
SLC43A3	3160.404972	0.6393	0.2405	0.0004	0.0363
STAT1	2377.08624	-0.7457	0.3277	0.0008	0.0453
STX16	956.6470281	-0.6724	0.1854	0.0000	0.0102
TAPBP	2418.783641	-0.6273	0.2170	0.0002	0.0272
TMBIM4	6890.701946	0.5847	0.1732	0.0001	0.0166
TMC8	482.6882232	-0.9717	0.3693	0.0003	0.0274
TMEM123	21566.67719	0.6470	0.2244	0.0002	0.0272
TMEM30A	2832.842693	0.5810	0.1811	0.0001	0.0227
TRIB3	688.4571657	0.8449	0.3313	0.0005	0.0380
TRIM56	1043.163351	-0.6095	0.1917	0.0001	0.0227
TSPAN31	508.5359559	0.6713	0.2326	0.0002	0.0272
TSPAN8	1083.273206	2.1683	0.4992	0.0000	0.0019
VDAC1_VDAC3	5771.330482	0.5896	0.1818	0.0001	0.0227
VPS37B	512.0670494	-1.0833	0.2549	0.0000	0.0019
VRK3	1292.114279	-0.5827	0.1526	0.0000	0.0102
YME1L1	1022.841411	0.6577	0.2260	0.0002	0.0272

Supplementary Table 6. Gene Set Enrichment Analysis of VILI and AIH cohorts after bulk RNA sequencing

Supplementary Table 6 can be found as a separate supplementary document.

Supplementary Table 7. Differential Gene Expression Analysis of VILI and AIH cohorts after spatial transcriptomics experiment

Supplementary Table 7 can be found as a separate supplementary document.

Supplementary Table 8. Gene Set Enrichment Analysis of VILI and AIH cohort after spatial transcriptomics experiment

Supplementary Table 8 can be found as a separate supplementary document.

Supplementary Table 9. Cohort of patients with DI-AILH

Patient ID	Sex	Age	Drug	AST (U/L)	ALT (U/L)	GGT (U/L)	ALP (U/L)	Bilirubin TOT (umol/l)	Auto-antibodies
DI-AILH1	f	40	Infliximab	559	957	72	237	154.7	ANA, 1:80
DI-AILH2	f	68	Infliximab	680	1167	342	172	NA	Anti-dsDNA
DI-AILH3	f	70	Atorvastatin	851	626	215	161	31.1	ANA, 1:320
DI-AILH4	f	66	Atorvastatin	35	35	556	363	6.5	ASMA, 1:640

Abbreviations: f: female, AST: aspartate aminotransferase ALT: alanine aminotransferase, GGT: Gamma-glutamyltransferase ALP: alkaline phosphatase, NA: not available, TOT: total, ANA: anti-nuclear antibody, ASMA: anti-smooth muscle antibody

Supplementary Table 10. Morphological Evaluation of DI-AILH Samples

Patient ID	Time between symptoms and liver biopsy (days)	Metavir Staging	Ishak Grading Total	Ishak Grading	Interface hepatitis (0-4)	Confluent necrosis (0-6)	Focal lytic necrosis (0-4)	Degree of Portal inflammation (0-4)
DI-AILH1	14	F0	7	2+0+2+3	2	0	2	3
DI-AILH2	5	F0	6	2+0+2+2	2	0	2	2
DI-AILH3	26	F0	10	3+1+2+4	3	1	2	4
DI-AILH4	220	F0	4	1+0+0+3	1	0	0	3

Supplementary Table 11. SARS-CoV-2 Spike Glycoprotein Epitopes with Matched CDR3 sequence

Input_sequence	Match_sequence	Score	Epitope	Antigen	Patient
ASSTGGTEAF	ASTTGGTEAF	0.9837	KLNDLCFTNVYADSFVIR	surface glycoprotein [Severe acute respiratory syndrome coronavirus 2]	VILI1
ASSGAASYEQY	ASSAGASSYEQY	0.9744	DLPIGINITRFQTL*	surface glycoprotein [Severe acute respiratory syndrome coronavirus 2]	VILI1
ASSGAASYEQY	ASSAGAASYEQY	0.9837	DLPIGINITRFQTL*	surface glycoprotein [Severe acute respiratory syndrome coronavirus 2]	VILI1
ASSLIGDTQY	ASSLLGDTQY	0.9808	RSVASQSIIAYTMSL**	surface glycoprotein [Severe acute respiratory syndrome coronavirus 2]	VILI3
ASSLIGDTQY	ASSLIGETQY	0.9711	QYIKWPWYI	surface glycoprotein [Severe acute respiratory syndrome coronavirus 2]	VILI3
ASSLEGSSYNEQF	ASSLDGSSYNEQF	0.9712	VQPTESIVRFPNITNLCPF	surface glycoprotein [Severe acute respiratory syndrome coronavirus 2]	VILI3
ASSFGSTDTQY	ASSFGTTDTQY	0.9776	YLQPRTFLL	surface glycoprotein [Severe acute respiratory syndrome coronavirus 2]	VILI4
ASSQGQPQH	ASSSQGQPQH	0.9701	RSVASQSIIAYTMSL**	surface glycoprotein [Severe acute respiratory syndrome coronavirus 2]	VILI5
ASALGSNQPQH	ASSLGSNQPQH	0.9831	FGEVFNATRFASVY	surface glycoprotein [Severe acute respiratory syndrome coronavirus 2]	VILI5

* Same epitope amino acid sequence

** Same epitope amino acid sequence

Supplementary Table 12. T-Cell Clones of VILI #5 Liver Biopsy and Blood Sample

Supplementary Table 12 can be found as a separate supplementary document.

Supplementary Table 13. T-Cell Clones of VILI_F Liver Biopsy and Blood Sample from Different Time Points

Supplementary Table 13 can be found as a separate supplementary document.

Supplementary Table 14. Review of vaccine induced liver injury cases from literature

Supplementary Table 14 can be found as a separate supplementary document.

Supplementary Table 15. qPCR Primers

Gene	Forward Primer	Reverse Primer
RNF213	5'-GACAGAACTGCAGACCACCG-3'	5'-GGTGGCTGTTTCATTCTCTGG-3'
TSPAN8	5'-GGCGACAGGTATCCTAGGAGC-3'	5'-CAATCAGCAGCTCCATTGACC-3'
GAPDH	5'-AGGTGAAGGTCGGAGTCAACG-3'	5'-TGGAAGATGGTGATGGGATTT-3'

Supplementary Table 16. Reagents used in CODEX Experiment

Product	Company	Cat.No (#)	
Coverslip	Electron Microscopy Sciences	72204-01	
Poly-L-Lysine Solution	Sigma-Aldrich	P8920	
10X Buffer	Akoya Biosciences	7000001	
Assay Reagent	Akoya Biosciences	7000002	
Nuclear Stain	Akoya Biosciences	7000003	
Staining Kit	Akoya Biosciences	7000008	
Antibody Conjugation Kit	Akoya Biosciences	7000009	
Storage Buffer	Akoya Biosciences	232107	
96 well plate	Akoya Biosciences	7000006	
96 well plate seal	Akoya Biosciences	7000007	
Paraformaldehyde 16% Solution	Electron Microscopy Sciences	15710	
Amicon Ultra-0.5 Centrifugal Filter Unit	Merck	UFC505024	

Primary Antibody	Company	Cat.No (#)	Clone Number
Anti-Liver Arginase antibody EPR6672(B) - BSA and Azide free	Abcam	ab211961	EPR6672(B)
CD20-BX007 (L26)	Akoya Biosciences	PN 232175	L26
CD8-BX026 (C8/144B)	Akoya Biosciences	PN 232151	C8/144B
CD68-BX015 (KP1)	Akoya Biosciences	PN 232176	KP1
CD4-BX003 (EPR6855)	Akoya Biosciences	PN 232174	EPR6855
CD3e-BX045 (EP449E)	Akoya Biosciences	PN 240006	EP449E
CD79a (JCB117) Mouse Monoclonal Antibody	Abcam	ab239891	EP3618
Ki67-BX047(B56)	Akoya Bioscience	PN 232179	B56
CD31-BX001 (EP3095)	Akoya Bioscience	PN 232172	EP3095
Purified anti-Cytokeratin 19 Antibody	Biolegend	628502	A53-B/A2
Purified anti-mouse/rat/human FOXP3 Antibody	Biolegend	320002	150D

Supplementary References

1. **Boettler T., Csernalabics B.**, Salie H., Luxenburger H., Wischer L., Alizei E.S., et al. SARS-CoV-2 vaccination can elicit a CD8 T-cell dominant hepatitis. *J Hepatol* 2022.
2. **Fontana R.J.**, Seeff L.B., Andrade R.J., Björnsson E., Day C.P., Serrano J., et al. Standardization of nomenclature and causality assessment in drug-induced liver injury: summary of a clinical research workshop. *Hepatology* 2010;52:730-42.
3. **Tiniakos D.G.**, Brain J.G., Bury Y.A. Role of Histopathology in Autoimmune Hepatitis. *Dig Dis* 2015;33 Suppl 2:53-64.
4. **Ishak K.**, Baptista A., Bianchi L., Callea F., Groote J.D., Gudat F., et al. Histological grading and staging of chronic hepatitis. *J Hepatol* 1995;22:696-9.
5. **Lohse A.W.**, Sebode M., Bhathal P.S., Clouston A.D., Dienes H.P., Jain D., et al. Consensus recommendations for histological criteria of autoimmune hepatitis from the International AIH Pathology Group: Results of a workshop on AIH histology hosted by the European Reference Network on Hepatological Diseases and the European Society of Pathology: Results of a workshop on AIH histology hosted by the European Reference Network on Hepatological Diseases and the European Society of Pathology. *Liver Int* 2022;42:1058-1069.
6. **Qu L.M.**, Wang S.H. Yang K., Brigstock D.R., Sun L., Gao R. et al. CD4(+)Foxp3(+)CD25(+/-) Tregs characterize liver tissue specimens of patients suffering from drug-induced autoimmune hepatitis: A clinical-pathological study. *Hepatobiliary Pancreat Dis Int* 2018;17:133-139.
7. **Love M.I.**, Huber W., Anders S. Moderated estimation of fold change and dispersion for RNA-seq data with DESeq2. *Genome Biol* 2014;15:550.
8. **Zhu A.**, Ibrahim J.G., Love M.I. Heavy-tailed prior distributions for sequence count data: removing the noise and preserving large differences. *Bioinformatics* 2019;35:2084-2092.
9. **Livak K.J.**, Schmittgen T.D. Analysis of relative gene expression data using real-time quantitative PCR and the 2(-Delta Delta C(T)) Method. *Methods* 2001;25:402-8.
10. **Merritt C.R.**, Ong G.T., Church S.E., Barker K., Danaher P., Geiss G., et al. Multiplex digital spatial profiling of proteins and RNA in fixed tissue. *Nat Biotechnol* 2020;38:586-599.
11. **Casarrubios M., Cruz-Bermudez A.**, Nadal E., Insa A., Campelo M.D.R.G, Lazaro M., et al. Pretreatment Tissue TCR Repertoire Evenness Is Associated with Complete Pathologic Response in Patients with NSCLC Receiving Neoadjuvant Chemoimmunotherapy. *Clin Cancer Res* 2021;27:5878-5890.

12. **Zhang J., Ji Z., Caushi J.X., Asmar M.E.,** Anagnostou V., Cottrell T.R., et al. Compartmental Analysis of T-cell Clonal Dynamics as a Function of Pathologic Response to Neoadjuvant PD-1 Blockade in Resectable Non-Small Cell Lung Cancer. Clin Cancer Res 2020;26:1327-1337.
13. Van der Loo M. The stringdist package for approximate string matching. The R Journal, 6, 111-122, <https://CRAN.R-project.org/package=stringdist> 2014.
14. Wickham H. ggplot2: Elegant Graphics for Data Analysis. Springer-Verlag New York. ISBN 978-3-319-24277-4. <https://ggplot2.tidyverse.org> 2016.
15. **Schindelin J.,** Arganda-Carreras I., Frise E., Kaynig V., Longair M., Pietzsch T., et al. Fiji: an open-source platform for biological-image analysis. Nat Methods 2012;9:676-82.
16. **Thevenaz P.,** Ruttimann U.E., Unser M. A pyramid approach to subpixel registration based on intensity. IEEE Trans Image Process 1998;7:27-41.
17. **Preibisch S.,** Saalfeld S., Tomancak P. Globally optimal stitching of tiled 3D microscopic image acquisitions. Bioinformatics 2009;25:1463-5.
18. **Guiet R.,** Burri O., Chiaruttini N., Seitz A., Eglinger J. Kheops (Version 0.1.8) [Computer software]. <https://doi.org/10.5281/zenodo.5256256> 2021.
19. **Bankhead P.,** Loughrey M.B., Fernández J.A., Dombrowski Y., McArt D.G., Dunne P.D., et al. QuPath: Open source software for digital pathology image analysis. Scientific Reports 2017;7:16878.
20. **Uhlen M.,** Fagerberg L., Hallstrom B.M., Lindskog C., Oksvold P., Mrdinoglu A., et al. Proteomics. Tissue-based map of the human proteome. Science 2015;347:1260419.
21. **Schmidt U.,** Weigert M., Broaddus C., Myers G. (2018). Cell Detection with Star-Convex Polygons. MICCAI 2018. Lecture Notes in Computer Science, vol 11071. Springer, Cham. 2018.
22. **Levine J.H., Simonds E.F., Bendall S.C.,** Davis K.L., Amir E.D., Tadmor M.D., et al. Data-Driven Phenotypic Dissection of AML Reveals Progenitor-like Cells that Correlate with Prognosis. Cell 2015;162:184-97.